

# Gravitational waves and Higgs boson couplings for exploring first order phase transition in the model with a singlet scalar field

Katsuya Hashino,<sup>1,\*</sup> Mitsuru Kakizaki,<sup>1,†</sup> Shinya Kanemura,<sup>1,‡</sup>

Pyungwon Ko,<sup>2,§</sup> and Toshinori Matsui<sup>2,¶</sup>

<sup>1</sup> *Department of Physics, University of Toyama,  
3190 Gofuku, Toyama 930-8555, Japan*

<sup>2</sup> *School of Physics, KIAS, Seoul 02455, Korea*

## Abstract

We calculate the spectrum of gravitational waves originated from strongly first order electroweak phase transition in the extended Higgs model with a real singlet field. In order to calculate the bubble nucleation rate, we perform a two-field analysis to evaluate bounce solutions connecting the true and the false vacua using the one-loop effective potential at finite temperatures. Imposing the Sakharov condition of the departure from thermal equilibrium for baryogenesis, we survey allowed regions of parameters of the model. We then investigate the gravitational waves produced at electroweak bubble collisions in the early Universe, such as the sound wave, the bubble wall collision and the plasma turbulence. We find that the strength at the peak frequency can be large enough to be detected at future space-based gravitational interferometers such as eLISA, DECIGO and BBO. Predicted deviations in the various Higgs boson couplings are also evaluated at the zero temperature, and are shown to be large enough too. Therefore, in this model strongly first order electroweak phase transition can be tested by the combination of the precision study of various Higgs boson couplings at LHC, the measurement of the triple Higgs boson coupling at future lepton colliders and the shape of the spectrum of gravitational wave detectable at future gravitational interferometers.

---

\*Electronic address: hashino@jodo.sci.u-toyama.ac.jp

†Electronic address: kakizaki@sci.u-toyama.ac.jp

‡Electronic address: kanemu@sci.u-toyama.ac.jp

§Electronic address: pko@kias.re.kr

¶Electronic address: matsui@kias.re.kr

By the discovery of a Higgs boson [1, 2] and the dedicated measurements of its property at LHC, the mass generation mechanism for elementary particles in the standard model (SM) has been established. One of the next important targets of high energy physics is to explore the structure of the Higgs sector, dynamics of electroweak symmetry breaking (EWSB), and the nature of the Higgs boson ( $h$ ).

In addition, the mechanism of electroweak phase transition (EWPT) is still a mystery, that is strongly related not only to the physics behind EWSB but also to various cosmological problems such as baryon asymmetry of the Universe and cosmic inflation. In particular, the strongly first order phase transition (1stOPT) is crucial for a successful scenario of electroweak baryogenesis (EWBG) [3]. With another requirement of additional CP violating phase, the EWBG scenario can be realized by introducing an extended Higgs sector. Therefore, in this scenario, the physics of EWBG can be in principle tested by exploring the Higgs sector.

It has been well known that the 1stOPT is realized by the non-decoupling thermal loop effects on the finite temperature effective potential and/or by the field mixing of the Higgs boson with additional scalar fields [4–25]. These effects also affect the effective potential at the zero temperature, so that they normally deviate the triple Higgs boson coupling (the  $hhh$  coupling) typically by larger than 10% [6, 10–12, 16, 17, 24–26]. It may be challenging for the (high luminosity) LHC to achieve this level of accuracy. However, the plan of the International Linear Collider (ILC) [27] includes the determination of the  $hhh$  coupling with 10% accuracy by upgrading the center-of-mass energy to  $\sqrt{s} = 1$  TeV [28–30]. The Compact Linear Collider (CLIC) [31] also aims to reach the similar accuracy. The Future Circular Collider of electrons and positrons (FCC-ee) [32] will not address the precision measurement of the  $hhh$  coupling as its center-of-mass energy is insufficient. The possibility of testing the  $hhh$  coupling at future hadron colliders with  $\sqrt{s} = 100$  TeV is also considered [33]. Therefore, the scenario of EWBG can be tested by precision measurements of the  $hhh$  coupling at future collider experiments. In a class of models where the 1stOPT is caused by the field mixing, resulting predicted values for the Higgs boson couplings such as those with weak gauge bosons and with fermions can also be deviated significantly because of the field mixing. Therefore, this class of models for EWBG is expected to be tested by the data from LHC not only those at future linear colliders.

On the other hand, it has also been known that strongly 1stOPT at the early Universe is

a discriminative origin of gravitational waves (GWs) [24, 25, 34–38]. Recently, the GWs has been directly detected at the Advanced LIGO experiment which has an astronomical origin [39]. By this discovery, measurements of GWs with various frequencies will be accelerated in the near future including KAGRA [40], Advanced LIGO [41] and Advanced VIRGO [42], by which new field of GW astronomy will be extensively developed. Furthermore, future space based GW interferometers such as eLISA [43], DECIGO [44] and BBO [45] provide us an opportunity of measuring GWs with a wider range of frequencies, which can cover GWs from the first order EWPT. Therefore, by precisely measuring the spectrum of GWs, we can test the physics of EWPT and further the scenario of EWBG.

In this Letter, we calculate the spectrum of GWs originated from strongly first order EWPT in a concrete renormalizable model, the extended Higgs model with a real singlet field. In order to calculate the bubble nucleation rate, we perform a two-field analysis to evaluate bounce solutions connecting the true and the false vacua using the one-loop effective potential at finite temperatures. We survey allowed regions of parameters of the model imposing the Sakharov condition of the departure from thermal equilibrium for baryogenesis [46]. We then investigate the GWs produced at electroweak bubble collisions in the early Universe, such as the sound wave, the bubble wall collision and the plasma turbulence. We find that in this model strongly first order EWPT can be well tested by the combination of the precision study of various Higgs boson couplings at LHC, the measurement of the  $hhh$  coupling at future lepton colliders and the spectrum of GWs detectable at eLISA and DECIGO.

Let us begin with a brief review of the Higgs singlet model (HSM), which is one of the simplest extensions of the SM [9, 10, 18, 47–51]. The Higgs sector of the HSM is equipped with a real isospin scalar singlet  $S$  in addition to the Higgs doublet  $\Phi$ . The general tree-level Higgs potential allowed by gauge invariance and renormalizability is given by

$$V_0 = -\mu_\Phi^2 |\Phi|^2 + \lambda_\Phi |\Phi|^4 + \mu_{\Phi S} |\Phi|^2 S + \frac{\lambda_{\Phi S}}{2} |\Phi|^2 S^2 + \mu_S^3 S + \frac{m_S^2}{2} S^2 + \frac{\mu'_S}{3} S^3 + \frac{\lambda_S}{4} S^4, \quad (1)$$

with eight parameters  $\mu_\Phi^2, m_S^2, \lambda_\Phi, \lambda_S, \lambda_{\Phi S}, \mu_{\Phi S}, \mu'_S$  and  $\mu_S^3$ .<sup>1</sup> After the condensation of the

---

<sup>1</sup> One of the mass parameters can be removed by the field redefinition of the singlet field without loss of generality [48, 49].

two Higgs fields, they are expanded around the vacuum expectation values  $v_\Phi$  and  $v_S$  as

$$\Phi = \begin{pmatrix} G^+ \\ \frac{1}{\sqrt{2}}(v_\Phi + \phi_1 + iG^0) \end{pmatrix}, \quad S = v_S + \phi_2. \quad (2)$$

There appear two physical degrees of freedom  $\phi_1$  and  $\phi_2$  that mix with each other in addition to Nambu-Goldstone (NG) modes  $G^\pm$  and  $G^0$  that are absorbed by the  $W$ - and  $Z$ -bosons. In the following, we analyze the phase structure of this HSM in the classical field space spanned by

$$\langle \Phi \rangle = \begin{pmatrix} 0 \\ \frac{1}{\sqrt{2}}\varphi_\Phi \end{pmatrix}, \quad \langle S \rangle = \varphi_S. \quad (3)$$

Radiative corrections modify the shape of the Higgs potential from the tree-level form. At zero temperature, the effective potential up to the one-loop level is [52]

$$V_{\text{eff}, T=0}(\varphi_\Phi, \varphi_S) = V_0(\varphi_\Phi, \varphi_S) + \sum_i n_i \frac{M_i^4(\varphi_\Phi, \varphi_S)}{64\pi^2} \left( \ln \frac{M_i^2(\varphi_\Phi, \varphi_S)}{Q^2} - c_i \right), \quad (4)$$

where  $Q$  is the renormalization scale, which is set at  $v_\Phi$  in our analysis. Here,  $n_i$  and  $M_i(\varphi_\Phi, \varphi_S)$  denote the degrees of the freedom and the field-dependent masses for particles  $i$ , respectively. We take the  $\overline{\text{MS}}$  scheme, where the numerical constants  $c_i$  are set at  $3/2$  ( $5/6$ ) for scalars and fermions (gauge bosons). We impose the tadpole conditions using the one-loop level effective potential as  $\langle \partial V_{\text{eff}, T=0} / \partial \varphi_i \rangle = 0$ , with  $i = \Phi$  or  $S$ . Here, the angle bracket  $\langle \cdots \rangle$  represents the field-dependent quantity evaluated at our true vacuum  $(\varphi_\Phi, \varphi_S) = (v_\Phi, v_S)$ . The mass squared matrix of the real scalar bosons in the  $(\phi_1, \phi_2)$  basis is diagonalized as

$$m_{ij}^2 = \left\langle \frac{\partial^2 V_{\text{eff}, T=0}}{\partial \varphi_i \partial \varphi_j} \right\rangle = \begin{pmatrix} \cos \theta & -\sin \theta \\ \sin \theta & \cos \theta \end{pmatrix} \begin{pmatrix} m_h^2 & 0 \\ 0 & m_H^2 \end{pmatrix} \begin{pmatrix} \cos \theta & \sin \theta \\ -\sin \theta & \cos \theta \end{pmatrix}, \quad (5)$$

leading to one-loop improved mass eigenvalues of the Higgs bosons  $m_h$  and  $m_H$ , and mixing angle  $\theta$  ( $m_h < m_H$ ,  $-\pi/4 \leq \theta \leq \pi/4$ ). The lighter boson  $h$  is identified with the discovered Higgs boson with the mass 125GeV in this Letter, and the alternative case where  $H$  is the discovered one will be examined elsewhere. From the above equations, we use  $v_\Phi$ ,  $v_S$ ,  $m_h$ ,

$m_H$  and  $\theta$  as the input parameters instead of  $\mu_\Phi^2$ ,  $m_S^2$ ,  $\lambda_\Phi$ ,  $\mu_{\Phi S}$  and  $\mu'_S$ .

Due to finite temperature effects, the effective potential is modified to [53]

$$V_{\text{eff},T}[M_i^2(\varphi_\Phi, \varphi_S)] = V_{\text{eff},T=0}(\varphi_\Phi, \varphi_S) + \sum_i n_i \frac{T^4}{2\pi^2} I_{B,F} \left( \frac{M_i^2(\varphi_\Phi, \varphi_S)}{T^2} \right), \quad (6)$$

where

$$I_{B,F}(a^2) = \int_0^\infty dx \, x^2 \ln \left( 1 \mp \exp^{-\sqrt{x^2+a^2}} \right), \quad (7)$$

for boson and fermions, respectively. In order to take ring-diagram contributions into account, we replace the field-dependent masses in the effective potential as [54]

$$M_i^2(\varphi_\Phi, \varphi_S) \rightarrow M_i^2(\varphi_\Phi, \varphi_S, T) = M_i^2(\varphi_\Phi, \varphi_S) + \Pi_i(T), \quad (8)$$

where  $\Pi_i(T)$  stand for the finite temperature contributions to the self energies. We consider loop contributions from the fields  $i = h, G^\pm, G^0, H, W_{T,L}^\pm, Z_{T,L}, \gamma_{T,L}, t$  and  $b$ . As for the scalar sector particles, the thermally corrected field-dependent masses are given by [47]

$$M_{h,H}^2(\varphi_\Phi, \varphi_S, T) = \frac{1}{2} \left( M_{11}^2 + M_{22}^2 \mp \sqrt{(M_{11}^2 - M_{22}^2)^2 + 4M_{12}^2 M_{21}^2} \right), \quad (9)$$

$$\begin{aligned} M_{G^0, G^\pm}^2(\varphi_\Phi, \varphi_S, T) = & -\mu_\Phi^2 + \lambda_\Phi \varphi_\Phi^2 + \mu_{\Phi S} \varphi_S + \frac{\lambda_{\Phi S}}{2} \varphi_S^2 \\ & + \frac{T^2}{48} (9g^2 + 3g'^2 + 12(y_t^2 + y_b^2) + 24\lambda_\Phi + 2\lambda_{\Phi S}), \end{aligned} \quad (10)$$

where

$$\begin{aligned} \begin{pmatrix} M_{11}^2 & M_{12}^2 \\ M_{21}^2 & M_{22}^2 \end{pmatrix} = & \begin{pmatrix} -\mu_\Phi^2 + 3\lambda_\Phi \varphi_\Phi^2 + \mu_{\Phi S} \varphi_S + \frac{\lambda_{\Phi S}}{2} \varphi_S^2 & \mu_{\Phi S} \varphi_\Phi + \lambda_{\Phi S} \varphi_\Phi \varphi_S \\ \mu_{\Phi S} \varphi_\Phi + \lambda_{\Phi S} \varphi_\Phi \varphi_S & m_S^2 + 2\mu'_S \varphi_S + 3\lambda_S \varphi_S^2 + \frac{\lambda_{\Phi S}}{2} \varphi_\Phi^2 \end{pmatrix} \\ & + \frac{T^2}{48} \begin{pmatrix} 9g^2 + 3g'^2 + 12(y_t^2 + y_b^2) + 24\lambda_\Phi + 2\lambda_{\Phi S} & 0 \\ 0 & 12\lambda_S + 8\lambda_{\Phi S} \end{pmatrix}. \end{aligned} \quad (11)$$

Here,  $g$  and  $g'$  ( $y_t$  and  $y_b$ ) represent the  $SU(2)$ ,  $U(1)$  gauge coupling constants (the top and bottom Yukawa coupling constants). For the thermal corrections to the field-dependent masses of the EW gauge bosons, see, for example, Ref. [25]. On the other hand, fermion

counterparts do not receive such thermal corrections.

Before analyzing the phase structure utilizing the finite temperature effective potential, let us briefly summarize important theoretical and experimental constraints on the HSM. In order to retain perturbative unitarity, the absolute values of eigenvalues of  $S$ -wave scattering amplitudes for the weak gauge bosons and scalars should be smaller than  $1/2$  [55]. This constraint is converted to the inequality  $m_h^2 \cos^2 \theta + m_H^2 \sin^2 \theta \leq 4\pi\sqrt{2}/(3G_F) \simeq (700 \text{ GeV})^2$ . Since  $m_h$  has been measured, an upper bound on the mixing angle  $\theta$  is obtained as a function of  $m_H$ . In order for the Higgs potential to be bounded from below, the vacuum stability condition has to be satisfied at a scale  $\mu$  [18]:

$$\lambda_\Phi(\mu) > 0, \quad \lambda_S(\mu) > 0, \quad 4\lambda_\Phi(\mu)\lambda_S(\mu) > \lambda_{\Phi S}^2(\mu). \quad (12)$$

It should be also noticed that in general the Higgs potential has several local minima. In order to prevent our EW phase from decaying into another one, the EW phase needs to be the global minimum of the Higgs potential as [49]

$$V_{\text{eff}, T=0}(\text{EW phase}) < V_{\text{eff}, T=0}(\text{other phases}). \quad (13)$$

Although the couplings in the Higgs potential remain perturbative at the EW scale, they become strong at higher energy scales due to renormalization group flow. In this Letter, the Landau pole  $\Lambda$  is defined as the scale where any of the Higgs couplings is as strong as  $|\lambda_{\Phi, S, \Phi S}(\Lambda)| = 4\pi$  [51]. For the HSM with strongly 1stOPT, the Landau pole ranges typically from a few TeV to around 10 TeV depending on parameter choices [18]. The introduction of the scalar singlet  $S$  also affects the self-energies of the  $W$ - and  $Z$ -bosons. For the details of the computations of the oblique parameters, see Ref. [56]. Given the observed value of the Higgs boson mass  $m_h \simeq 125 \text{ GeV}$ , the Higgs boson mixing angle is constrained as  $\cos \theta \gtrsim 0.92$  for  $m_H \gtrsim 400 \text{ GeV}$  [57].

The presence of the scalar singlet gives rise to deviations in the couplings of the discovered Higgs boson from their SM values. The dominant contributions to the deviations are induced by the mixing between the two Higgs bosons. Therefore, the predicted Higgs boson couplings to the gauge boson  $V = W^\pm, Z$  and fermions  $F$  normalized by the corresponding SM ones are universal as  $\kappa = \kappa_V = \kappa_F = \cos \theta$ . The most stringent bounds are extracted from

the measurements of the Higgs boson decay into weak gauge bosons at the LHC Run-I as  $\kappa_Z = 1.03^{+0.11}_{-0.11}$ ,  $\kappa_W = 0.91^{+0.10}_{-0.10}$  [58]. The high-luminosity stage of the LHC can reach the precision of 2% [59]. The precision of the Higgs boson coupling measurements will be significantly improved once electron-positron colliders are realized. In the case of the ILC with  $\sqrt{s} = 500$  GeV, the expected accuracy can be 0.37% (0.51%) for  $\kappa_Z$  ( $\kappa_W$ ) [30].

The value of the  $hhh$  coupling  $\lambda_{hhh}$  is considerably altered by the new singlet scalar. Here, for simplicity, we adopt the effective potential approach in computing  $\lambda_{hhh}$ .<sup>2</sup> In this approximation, the SM prediction is obtained as

$$\lambda_{hhh}^{\text{SM}} = \frac{3m_h^2}{v_\Phi} \left[ 1 + \frac{9m_h^2}{32\pi^2 v_\Phi^2} + \sum_{i=W^\pm, Z, t, b} n_i \frac{m_i^4}{12\pi^2 m_h^2 v_\Phi^2} \right] \simeq 176 \text{ GeV}, \quad (14)$$

while the HSM counterpart is symbolically expressed as<sup>3</sup>

$$\lambda_{hhh}^{\text{HSM}} = c_\theta^3 \left\langle \frac{\partial^3 V_{\text{eff}, T=0}}{\partial \varphi_\Phi^3} \right\rangle + c_\theta^2 s_\theta \left\langle \frac{\partial^3 V_{\text{eff}, T=0}}{\partial \varphi_\Phi^2 \partial \varphi_S} \right\rangle + c_\theta s_\theta^2 \left\langle \frac{\partial^3 V_{\text{eff}, T=0}}{\partial \varphi_\Phi \partial \varphi_S^2} \right\rangle + s_\theta^3 \left\langle \frac{\partial^3 V_{\text{eff}, T=0}}{\partial \varphi_S^3} \right\rangle, \quad (15)$$

where  $c_\theta = \cos \theta$  and  $s_\theta = \sin \theta$ . In discussing the deviation in the  $hhh$  coupling, we exclusively utilize the following normalized quantity:

$$\Delta \lambda_{hhh} = \frac{\lambda_{hhh}^{\text{HSM}} - \lambda_{hhh}^{\text{SM}}}{\lambda_{hhh}^{\text{SM}}}. \quad (16)$$

So far, the LHC has set no meaningful constraint on the  $hhh$  coupling. In the future, at the high luminosity LHC with  $L = 3000 \text{ fb}^{-1}$  the production cross section of the double Higgs production process can be measured with 54% [62]. Once realized, the ILC is capable of measuring the  $hhh$  coupling with considerable accuracy. The ILC stage with  $\sqrt{s} = 500$  GeV and  $L = 4000 \text{ fb}^{-1}$ , the expected precision is 27% [30]. At the ILC with the higher energy of  $\sqrt{s} = 1$  TeV, the precision will be ameliorated to 16% (10%) for  $L = 2000 \text{ fb}^{-1}$  ( $L = 5000 \text{ fb}^{-1}$ ) [30].

Let us consider the EWPT in the HSM. In order for baryogenesis to work, the departure from thermal equilibrium must be realized. In EWBG scenarios, the baryon number chang-

---

<sup>2</sup> Dependence of the  $hhh$  coupling on the external momentum is discussed in Refs. [60, 61].

<sup>3</sup> In our analysis at zero temperature, we disregard the minor loop contributions from the NG modes in order to avoid complexity.

ing sphaleron process must decouple quickly after the EWSB: the sphaleron interaction rate  $\Gamma_{\text{sph}}(T)$  is smaller than the Hubble expansion rate  $H(T)$ . This criterion is satisfied if the EWSB is of strongly first order

$$\frac{\varphi_c}{T_c} > \zeta_{\text{sph}}(T_c), \quad (17)$$

where  $\varphi_c$  is the VEV for the true vacuum at the critical temperature  $T_c$ . The value of  $\zeta_{\text{sph}}(T_c)$  is typically around unity, and it is estimated as  $\zeta_{\text{sph}}(T_c) = 1.1 - 1.2$  for the HSM [18].

Let us turn our discussion to GWs originated from the first order EWPT in the HSM. First, we introduce two important quantities  $\alpha$  and  $\beta$  that describe the dynamics of vacuum bubbles [35]. First, we define the transition temperature such that the bubble nucleation probability per Hubble volume per Hubble time reaches the unity,  $\Gamma/H^4|_{T=T_t} = 1$ . The parameter  $\alpha$  is the ratio of the released energy density  $\epsilon$  to the radiation energy density  $\rho_{\text{rad}} = (\pi^2/30)g_*T^4$  at the transition temperature  $T_t$ :

$$\alpha \equiv \frac{\epsilon(T_t)}{\rho_{\text{rad}}(T_t)}. \quad (18)$$

In our analysis, for simplicity, we neglect the temperature dependence of the relativistic degrees of freedom, and fix it at  $g_* = 107.65$ . The parameter  $\beta$  is the inverse of the time variation scale of the bubble nucleation rate  $\Gamma(t) = \Gamma_0 \exp(\beta t)$ . It is a standard to use the normalized dimensionless parameter  $\tilde{\beta}$ , which is defined as

$$\tilde{\beta} \equiv \frac{\beta}{H_t} = T_t \frac{d}{dT} \left( \frac{S_3(T)}{T} \right) \Big|_{T=T_t}, \quad (19)$$

where  $S_3(T)$  is the three dimensional Euclidean action for the bounce configuration of the classical field that connects the true and the false vacua at  $T$ . Once  $T_t$ ,  $\alpha$  and  $\beta$  are computed, one can estimate the spectrum of the stochastic GWs using the approximate analytic formula provided in Ref. [37].

We are now at the stage of discussing the testability of the HSM by utilizing the interplay of measurements of Higgs boson couplings at future colliders and of GWs at future space-based interferometers. In the light of the constraints on the HSM discussed above, we perform numerical analysis in computing the Higgs boson couplings and bubble dynamics



TABLE I: The benchmark point and scanned range for the HSM parameters.

$v_\Phi$ [GeV]	$v_S$ [GeV]	$m_h$ [GeV]	$\mu_{\Phi S}$ [GeV]	$\mu'_S$ [GeV]	$\mu_S$ [GeV]	$m_H$ [GeV]	$\theta$ [degrees]
246.2	90	125.5	-80	-30	0	[160, 240]	[-45, 0]

parameters. The characteristic feature of the HSM (without  $Z_2$  symmetry) is that the potential barrier between the true and the false vacua necessary for 1stOPT can be formed mainly by tree-level interactions, in sharp contrast to the two Higgs doublet models or  $Z_2$  symmetric HSM, where non-decoupling loop effects are necessitated for 1stOPT. As an example scenario where strongly 1stOPT is accomplished due to large doublet-singlet Higgs mixing parameters  $\mu_{\Phi S}$  and  $\lambda_{\Phi S}$ , we consider the benchmark point shown in Table I <sup>4</sup>. In evaluating  $T_t, \alpha$  and  $\tilde{\beta}$ , we implement the HSM into the public code `CosmoTransitions` [63], which computes quantities related to the cosmological phase transition in the multi-field space. Predicted GW spectra are estimated using the approximate analytic formula developed in [37, 64].

In Fig. 1, we present the predicted values of  $\alpha$  and  $\beta$  with the variation of  $(m_H, -\theta)$ . in the HSM for the benchmark point in Table I. The black curves show the predicted values of  $\alpha$  and  $\beta$  for  $m_H = 180$  GeV, 200 GeV, 220 GeV and 240 GeV from the left. The upper bound on  $\tilde{\beta}$  is set by the condition  $\varphi_c/T_c = 1$ . Since  $S_3(T)/T$  is a concave function of  $T$ , not only positive but also negative values of  $\tilde{\beta}$  may be derived from the criterion  $\Gamma/H^4|_{T=T_t} = 1$  due to a naive numerical analysis [34, 38]. In this Letter, we just remove such cases from our plot because our conclusion is not affected. The lower end of each black curve is drawn by this procedure. The shaded regions represent the expected coverage at the future space-based interferometers, eLISA [37, 65, 66] and DECIGO [44]. The sensitivity regions of four eLISA detector configurations described in Table I in Ref. [37] are denoted by “C1”, “C2”, “C3” and “C4”. The expected sensitivities for the future DECIGO stages are labeled by “Correlation”, “1 cluster” and “Pre” following Ref. [44]. Although the transition temperature  $T_t$  depends on the HSM parameters, we take  $T_t = 50$  GeV for the purpose of illustration. The experimental sensitivities are also dependent on the velocity of the bubble wall  $v_b$ , which is uncertain. As a reference, we take  $v_b = 0.95$  so that strong GW signals are expected <sup>5</sup>. If we take smaller values of  $v_b$  such as 0.2, which the EWBG scenario prefers, the

<sup>4</sup> For the purpose of straightforward comparison, we take the same benchmark point as Case (ii) in Ref. [18].

<sup>5</sup> In Ref. [67], EWBG is not necessarily impossible even in this case.

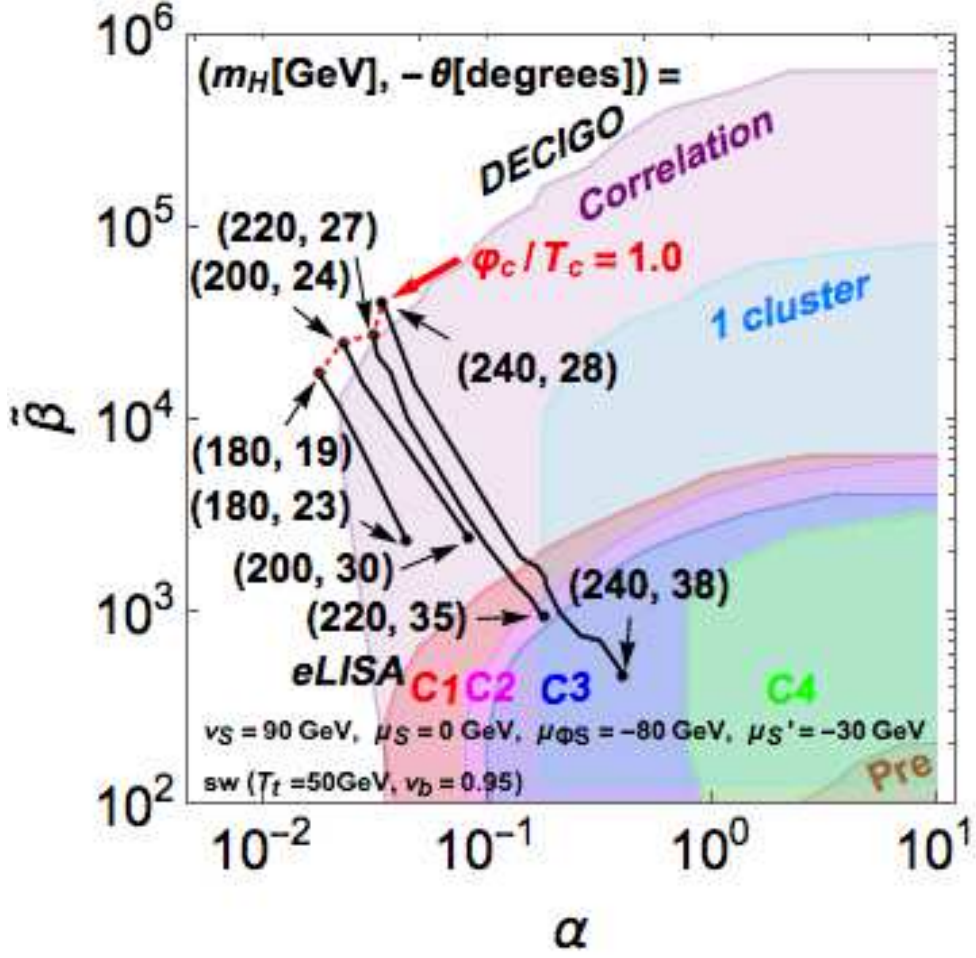


FIG. 1: The predicted values of  $\alpha$  and  $\tilde{\beta}$  with the variation of  $(m_H, -\theta)$  in the HSM for the benchmark point in Table I. The expected sensitivities of eLISA and DECIGO detector configurations are set by using the sound wave contribution for  $T_t = 50$  GeV and  $v_b = 0.95$ .

sensitivity area is pushed down to lower  $\tilde{\beta}$  and larger  $\alpha$  regions. For  $v_b < 1$ , the contribution from the sound waves is the dominant source of the total GW spectrum while those from the bubble wall collision and the turbulence are not significant [68]. This plot demonstrates that eLISA or DECIGO is capable of detecting stochastic GWs from the sound wave source in the most of the HSM parameter region with 1stOPT.

In Fig. 2, the detectability of GWs and the contours of the deviation in the triple Higgs boson coupling  $\Delta\lambda_{hhh}$  in the HSM are shown in the  $m_H$ - $\kappa$  plane. The projected region of a higher sensitive detector design is overlaid with that of weaker one. The region which satisfies both  $\varphi_c/T_c > 1$  and  $T_c > 0$  is also shown for a reference. This plot highlights the importance of the synergy between the precision measurements of the Higgs boson couplings

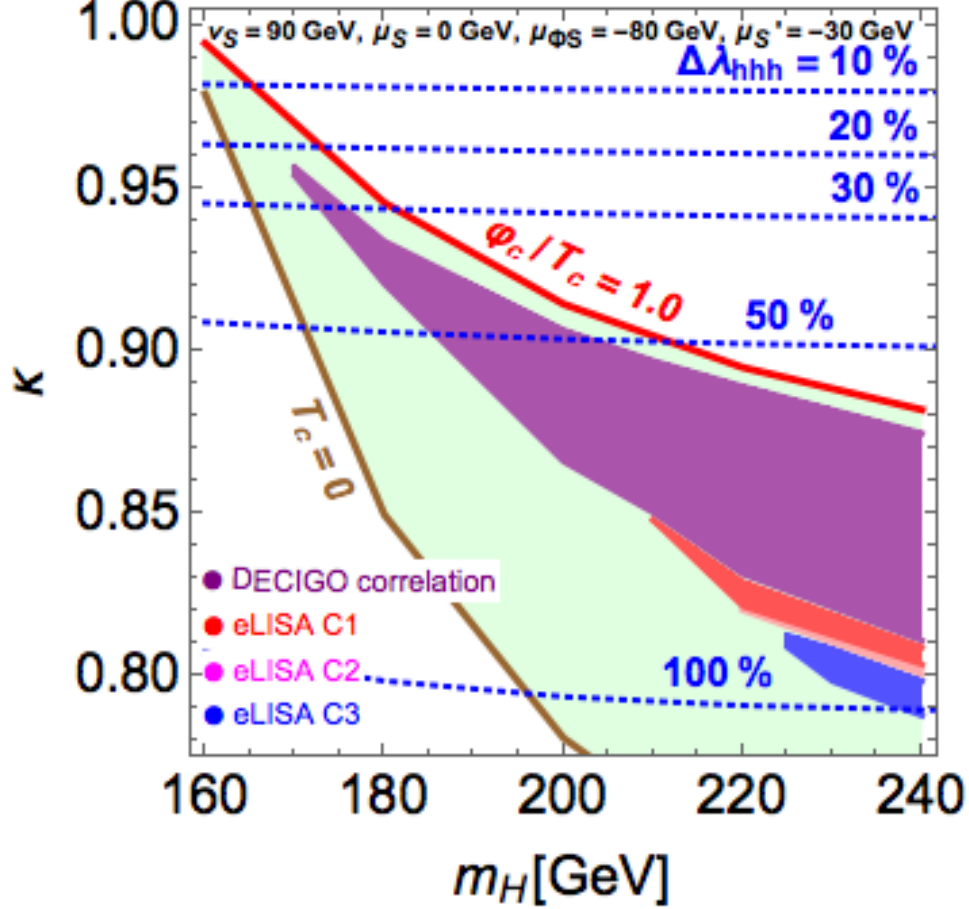


FIG. 2: The detectability of GWs and the contours of the deviations in the  $hhh$  coupling  $\Delta\lambda_{hhh}$  in the  $m_H$ - $\kappa$  plane. The projected region of a higher sensitive detector design is overlaid with that of weaker one. The region which satisfies both  $\varphi_c/T_c > 1$  and  $T_c > 0$  is also shown for a reference. The input parameters and legends are same as in Fig. 1

at future colliders and the observation of stochastic GWs at future GW interferometers. As deviations in the Higgs boson couplings from the SM values are larger, the strength of 1stOPT and that of GW signals are more significant. For example, once  $\kappa$  is found to be smaller than 0.95 by LHC experiments, then the  $hhh$  coupling should be greater than 20%. Such a deviation in the  $hhh$  coupling can be measured at the ILC with  $\sqrt{s} = 1$  TeV [30]. In addition, we learn from Fig. 2 that the scenario can also be well tested at DECIGO and eLISA. The combined measurements make it possible to identify the shape of the Higgs potential of the HSM.

In this Letter, we have evaluated the spectrum of GWs that are generated from the strongly 1stOPT of the EWSB in the HSM. Based on the finite temperature one-loop

effective potential with the two scalar fields, the profile of the vacuum bubble and the transition temperature for the tunneling from the false vacuum to the true one have been analyzed. In view of EWBG, the parameter space allowed by the condition of the departure from thermal equilibrium has been explored. We have investigated the GW signals from the sound waves, the bubble wall collision and the turbulence resulting from the bubble collisions. We have pointed out that the predicted peak GW amplitude from the sound wave contribution is so strong as to be detected at future space-based interferometers such as eLISA, DECIGO and BBO. Deviations in the Higgs boson couplings have been also evaluated, and found to be measurable at future colliders. Therefore, we conclude that the strongly 1stOPT of EWSB in the HSM can be verified by combining the precision measurements of various Higgs boson couplings at the LHC and the  $hhh$  coupling at future electron-positron colliders with those of stochastic GW background at future space-based interferometers.

*Note Added:* During the completion of the manuscript, we became aware of an analogous calculation done independently by another group [69].

## Acknowledgments

This work was supported, in part, by Grant-in-Aid for Scientific Research on Innovative Areas, the Ministry of Education, Culture, Sports, Science and Technology, No. 16H01093 (MK) and No. 16H06492 (SK), Grant H2020-MSCA-RISE-2014 no. 645722 (Non Minimal Higgs) (SK), and National Research Foundation of Korea (NRF) Research Grant NRF-2015R1A2A1A05001869 (PK,TM).

- 
- [1] G. Aad *et al.* [ATLAS Collaboration], Phys. Lett. B **716**, 1 (2012).
  - [2] S. Chatrchyan *et al.* [CMS Collaboration], Phys. Lett. B **716**, 30 (2012).
  - [3] V. A. Kuzmin, V. A. Rubakov and M. E. Shaposhnikov, Phys. Lett. B **155**, 36 (1985).
  - [4] K. Funakubo, A. Kakuto and K. Takenaga, Prog. Theor. Phys. **91**, 341 (1994).
  - [5] J. M. Cline and P. A. Lemieux, Phys. Rev. D **55**, 3873 (1997).
  - [6] S. Kanemura, Y. Okada and E. Senaha, Phys. Lett. B **606**, 361 (2005).

- [7] K. Funakubo, S. Tao and F. Toyoda, *Prog. Theor. Phys.* **114**, 369 (2005).
- [8] J. R. Espinosa and M. Quiros, *Phys. Rev. D* **76**, 076004 (2007).
- [9] S. Profumo, M. J. Ramsey-Musolf and G. Shaughnessy, *JHEP* **0708**, 010 (2007).
- [10] A. Noble and M. Perelstein, *Phys. Rev. D* **78**, 063518 (2008).
- [11] M. Aoki, S. Kanemura and O. Seto, *Phys. Rev. Lett.* **102**, 051805 (2009); *Phys. Rev. D* **80**, 033007 (2009); M. Aoki, S. Kanemura and K. Yagyu, *Phys. Rev. D* **83**, 075016 (2011).
- [12] S. Kanemura, E. Senaha and T. Shindou, *Phys. Lett. B* **706**, 40 (2011).
- [13] G. Gil, P. Chankowski and M. Krawczyk, *Phys. Lett. B* **717**, 396 (2012).
- [14] M. Fairbairn and R. Hogan, *JHEP* **1309** (2013) 022.
- [15] T. Li and Y. F. Zhou, *JHEP* **1407**, 006 (2014).
- [16] C. Tamarit, *Phys. Rev. D* **90**, no. 5, 055024 (2014).
- [17] S. Kanemura, N. Machida and T. Shindou, *Phys. Lett. B* **738**, 178 (2014).
- [18] K. Fuyuto and E. Senaha, *Phys. Rev. D* **90**, no. 1, 015015 (2014).
- [19] S. Profumo, M. J. Ramsey-Musolf, C. L. Wainwright and P. Winslow, *Phys. Rev. D* **91**, no. 3, 035018 (2015).
- [20] W. Chao, *Phys. Rev. D* **92**, no. 1, 015025 (2015).
- [21] N. Blinov, S. Profumo and T. Stefaniak, *JCAP* **1507**, no. 07, 028 (2015).
- [22] K. Fuyuto and E. Senaha, *Phys. Lett. B* **747**, 152 (2015).
- [23] A. Karam and K. Tamvakis, *Phys. Rev. D* **92**, no. 7, 075010 (2015).
- [24] M. Kakizaki, S. Kanemura and T. Matsui, *Phys. Rev. D* **92**, no. 11, 115007 (2015).
- [25] K. Hashino, M. Kakizaki, S. Kanemura and T. Matsui, *Phys. Rev. D* **94**, no. 1, 015005 (2016).
- [26] K. Hashino, S. Kanemura and Y. Orikasa, *Phys. Lett. B* **752**, 217 (2016).
- [27] J. Brau, (Ed.) *et al.* [ILC Collaboration], arXiv:0712.1950 [physics.acc-ph]; G. Aarons *et al.* [ILC Collaboration], arXiv:0709.1893 [hep-ph]; N. Phinney, N. Toge and N. Walker, arXiv:0712.2361 [physics.acc-ph]; T. Behnke, (Ed.) *et al.* [ILC Collaboration], arXiv:0712.2356 [physics.ins-det]; T. Behnke *et al.*, arXiv:1306.6329 [physics.ins-det]; H. Baer, *et al.* "Physics at the International Linear Collider", *Physics Chapter of the ILC Detailed Baseline Design Report*: <http://lcsim.org/papers/DBDPhysics.pdf>.
- [28] D. M. Asner, T. Barklow, C. Calancha, K. Fujii, N. Graf, H. E. Haber, A. Ishikawa and S. Kanemura *et al.*, arXiv:1310.0763 [hep-ph].
- [29] G. Moortgat-Pick *et al.*, *Eur. Phys. J. C* **75**, no. 8, 371 (2015).

- [30] K. Fujii *et al.*, arXiv:1506.05992 [hep-ex].
- [31] E. Accomando *et al.* [CLIC Physics Working Group Collaboration], hep-ph/0412251; L. Linssen, A. Miyamoto, M. Stanitzki and H. Weerts, arXiv:1202.5940 [physics.ins-det].
- [32] M. Bicer *et al.* [TLEP Design Study Working Group Collaboration], JHEP **1401**, 164 (2014).
- [33] H. J. He, J. Ren and W. Yao, Phys. Rev. D **93**, no. 1, 015003 (2016).
- [34] R. Areda, M. Maggiore, A. Nicolis and A. Riotto, Nucl. Phys. B **631**, 342 (2002).
- [35] C. Grojean and G. Servant, Phys. Rev. D **75**, 043507 (2007).
- [36] J. R. Espinosa, T. Konstandin, J. M. No and M. Quiros, Phys. Rev. D **78**, 123528 (2008).
- [37] C. Caprini *et al.*, JCAP **1604**, no. 04, 001 (2016).
- [38] A. Kobakhidze, A. Manning and J. Yue, arXiv:1607.00883 [hep-ph].
- [39] B. P. Abbott *et al.* [LIGO Scientific and Virgo Collaborations], Phys. Rev. Lett. **116**, no. 6, 061102 (2016); Phys. Rev. Lett. **116**, no. 24, 241103 (2016).
- [40] K. Somiya [KAGRA Collaboration], Class. Quant. Grav. **29**, 124007 (2012).
- [41] G. M. Harry [LIGO Scientific Collaboration], Class. Quant. Grav. **27**, 084006 (2010).
- [42] T. Accadia *et al.*, Proceedings of *12th Marcel Grossmann Meeting on General Relativity*, pp. 1738–1742 (2009).
- [43] P. A. Seoane *et al.* [eLISA Collaboration], arXiv:1305.5720 [astro-ph.CO].
- [44] S. Kawamura *et al.*, Class. Quant. Grav. **28**, 094011 (2011).
- [45] V. Corbin and N. J. Cornish, Class. Quant. Grav. **23**, 2435 (2006).
- [46] A. D. Sakharov, Pisma Zh. Eksp. Teor. Fiz. **5**, 32 (1967).
- [47] A. Ashoorioon and T. Konstandin, JHEP **0907**, 086 (2009).
- [48] J. R. Espinosa, T. Konstandin and F. Riva, Nucl. Phys. B **854**, 592 (2012).
- [49] C. Y. Chen, S. Dawson and I. M. Lewis, Phys. Rev. D **91**, no. 3, 035015 (2015).
- [50] S. Kanemura, M. Kikuchi and K. Yagyu, Nucl. Phys. B **907**, 286 (2016)
- [51] S. Kanemura, M. Kikuchi and K. Yagyu, arXiv:1608.01582 [hep-ph].
- [52] S. R. Coleman and E. J. Weinberg, Phys. Rev. D **7**, 1888 (1973).
- [53] L. Dolan and R. Jackiw, Phys. Rev. D **9**, 3320 (1974).
- [54] M. E. Carrington, Phys. Rev. D **45**, 2933 (1992).
- [55] B. W. Lee, C. Quigg and H. B. Thacker, Phys. Rev. D **16**, 1519 (1977).
- [56] S. Baek, P. Ko and W. I. Park, JHEP **1202**, 047 (2012).
- [57] S. Baek, P. Ko, W. I. Park and E. Senaha, JHEP **1211**, 116 (2012).

- [58] The ATLAS and CMS Collaborations, ATLAS-CONF-2015-044.
- [59] CMS Collaboration, arXiv:1307.7135.
- [60] S. Kanemura, S. Kiyoura, Y. Okada, E. Senaha and C. P. Yuan, Phys. Lett. B **558**, 157 (2003).
- [61] S. Kanemura, Y. Okada, E. Senaha and C.-P. Yuan, Phys. Rev. D **70**, 115002 (2004).
- [62] CMS Collaboration CMS-PAS-FTR-15-002.
- [63] C. L. Wainwright, Comput. Phys. Commun. **183**, 2006 (2012).
- [64] J. R. Espinosa, T. Konstandin, J. M. No and G. Servant, JCAP **1006**, 028 (2010).
- [65] A. Klein *et al.*, Phys. Rev. D **93**, no. 2, 024003 (2016).
- [66] Data sheet by A. Petiteau,  
<http://www.apc.univ-paris7.fr/Downloads/lisa/eLISA/Sensitivity/Cfgv1/StochBkgd/>
- [67] J. M. No, Phys. Rev. D **84**, 124025 (2011).
- [68] M. Hindmarsh, S. J. Huber, K. Rummukainen and D. J. Weir, Phys. Rev. Lett. **112**, 041301 (2014); Phys. Rev. D **92**, no. 12, 123009 (2015).
- [69] P. Huang, A. J. Long and L. T. Wang, arXiv:1608.06619 [hep-ph].